Journal of Glaciology (2018), **64**(243) 37–48 doi: 10.1017/jog.2017.81

Assessing the applicability of terrestrial laser scanning for mapping englacial conduits

J. E. KAMINTZIS,[1] J. P. P. JONES,[2] T. D. L. IRVINE-FYNN,[1] T. O. HOLT,[1] P. BUNTING,[1] S. J. A. JENNINGS,[1] P. R. PORTER,[3] B. HUBBARD[1]

[1]*Department of Geography and Earth Sciences, Centre for Glaciology, Aberystwyth University, Aberystwyth, SY23 3DB, Wales, UK*
[2]*Deri Jones & Associates, Ltd., Machynlleth, Wales, UK*
[3]*School of Life and Medical Sciences, University of Hertfordshire, UK*
Correspondence: J.E. Kamintzis <jek12@aber.ac.uk>

ABSTRACT. The morphology of englacial drainage networks and their temporal evolution are poorly characterised, particularly within cold ice masses. At present, direct observations of englacial channels are restricted in both spatial and temporal resolution. Through novel use of a terrestrial laser scanning (TLS) system, the interior geometry of an englacial channel in Austre Brøggerbreen, Svalbard, was reconstructed and mapped. Twenty-eight laser scan surveys were conducted in March 2016, capturing the glacier surface around a moulin entrance and the uppermost 122 m reach of the adjoining conduit. The resulting point clouds provide detailed 3-D visualisation of the channel with point accuracy of 6.54 mm, despite low (<60%) overall laser returns as a result of the physical and optical properties of the clean ice, snow, hoar frost and sediment surfaces forming the conduit interior. These point clouds are used to map the conduit morphology, enabling extraction of millimetre-to-centimetre scale geometric measurements. The conduit meanders at a depth of 48 m, with a sinuosity of 2.7, exhibiting teardrop shaped cross-section morphology. This improvement upon traditional surveying techniques demonstrates the potential of TLS as an investigative tool to elucidate the nature of glacier hydrological networks, through reconstruction of channel geometry and wall composition.

KEYWORDS: arctic glaciology, glacier mapping, glaciological instruments and methods, remote sensing

1. INTRODUCTION

Englacial channels deliver surface meltwater to the interior and base of ice masses (Fountain and Walder, 1998; Irvine-Fynn and others, 2011). This delivery influences glacier mass balance as a result of its close association with ice dynamics (e.g. Iken and Bindschadler, 1986; Zwally and others, 2002; Mair, 2005; Schoof, 2010), water storage (Jansson and others, 2003; Lingle and Fatland, 2003) and thermal energy transfer within the glacier system (Phillips and others, 2010; Mankoff and Tulaczyk, 2017). Englacial drainage networks have been identified and described in temperate (e.g. Harper and Humphrey, 1995; Piccini and others, 2002; Gulley, 2009) and polythermal glaciers (e.g. Pulina, 1984; Holmlund, 1988; Moorman and Michel, 2000; Gulley and others, 2009a), with more recent observations highlighting the existence of englacial conduits in cold ice margins (Vatne, 2001; Benn and others, 2009; Gulley and others, 2009a; Bælum and Benn, 2011; Naegeli and others, 2014) and ice-sheet settings (Catania and others, 2008; Das and others, 2008). However, these conduits are difficult to access directly and, consequently, a process-level understanding of their geometry, formation and evolution remains poorly constrained (Vatne and Irvine-Fynn, 2016).

To date, knowledge of englacial hydrological systems has been inferred from borehole observations (Harper and Humphrey, 1995; Fountain and others, 2005), dye-tracing experiments (Willis and others, 1990; Nienow and others, 1998; Bingham and others, 2005; Irvine-Fynn and others, 2005) and geophysical surveys (Moorman and Michel, 2000; Stuart, 2003; Catania and others, 2008) or directly assessed with speleological explorations using traditional cave surveying techniques (Pulina, 1984; Vatne, 2001; Vatne and Refsnes, 2003; Gulley and others, 2009a,b). Although the last provides the only direct observations of the interior of englacial channels, the spatial resolution of these surveys are limited, with dimensional measurements and sketches of cross-section morphology being carried out at changes in channel orientation and inclination (Warild, 2007). In englacial channels, the intervals between such changes are typically on the order of several to tens of metres, meaning that such surveys provide sparse coverage over mapped reaches of up to hundreds of metres and, thus, provide little morphological detail. Given that channel morphology can alter over much smaller spatial scales, due to complex feedback mechanisms between morphology and flow dynamics, finer resolution surveys are required for enhancing understanding of englacial channel geometry and its temporal evolution across daily to decadal timescales.

Recent technological development, in the form of terrestrial laser scanning (TLS), provides an opportunity to improve upon these manual measurements of englacial morphology. In geomorphological and industrial settings, TLS is already an established tool for mapping of rock and ice-coated caves (Buchroithner and others, 2009; Cosso and others, 2014; Gallay and others, 2015; Idrees and Pradhan, 2016) and artificial tunnels (Li and others, 2012).

TLS enables rapid acquisition (minutes to hours) of high accuracy datasets at millimetre-scale spatial resolution, allowing for detailed retrospective measurements of target features to be made at fine spatial intervals (Lichti and others, 2002; Pfiefer and Briese, 2007). Within cryospheric research, TLS has been successfully used to recreate 3-D snow and ice surfaces, allowing determination of snow depth distributions (Jörg and others, 2006; Kaasalainen and others, 2008; Osterhuber and others, 2008; Prokop, 2008), glacier surface roughness (Smith and others, 2016), surface ablation (Gabbud and others, 2015) and mass balance (Fischer and others, 2016). Therefore, TLS could provide an innovative alternative to current glacio-speleological methods of cartography and morphological analysis. To our knowledge, a detailed morphological assessment of an englacial channel using TLS has yet to be undertaken, largely as a result of the challenges presented by the optical and physical properties of ice (Lichti and others, 2002) and the practicalities of using older TLS instruments in these more rugged environments.

Here, we describe the novel use of TLS technology to reconstruct the internal geometry of an englacial channel in the High Arctic glacier, Austre Brøggerbreen, detailing the practical survey methods and data processing techniques used to recreate and map conduit morphology. The results are used to evaluate the potential of TLS for mapping of ice-walled channels, as an improvement on traditional manual surveying for morphological analyses.

2. FIELD SITE AND DATA ACQUISITION

2.1. Field site

Austre Brøggerbreen is a 5 km long, predominantly cold-based, valley glacier located on the Brøggerhalvoya Peninsula, Svalbard (79° 55′ N, 11° 46′ E; Fig. 1). The glacier extends from ~50 to 600 m a.s.l., covering an area of ~9.4 km^2 with an ice thickness of <100 m, and comprising six flow units that feed into a relatively short tongue (Bruland and Hagen, 2002; Porter and others, 2010; Jennings and others, 2015). Low ice surface velocities of <3 m a^{-1} (Hagen and others, 1993), together with recent downwasting and recession (Barrand and others, 2010), have led to the transition of the glacier from a polythermal regime to a cold-based one (cf. Hagen and Sætrang, 1991; Björnsson and others, 1996; Nowak and Hodson, 2014). This change in thermal structure has facilitated the development of an extensive and stable supraglacial drainage network, with several deeply incised surface channels feeding into perennial moulins. Formation of englacial channels through cut-and-closure mechanisms form a substantial part of Austre Brøggerbreen's hydrological system (Vatne, 2001; Stuart, 2003; Vatne and Refsnes, 2003; Vatne and Irvine-Fynn, 2016), which drains through a main portal at the eastern glacier margin (Porter and others, 2010).

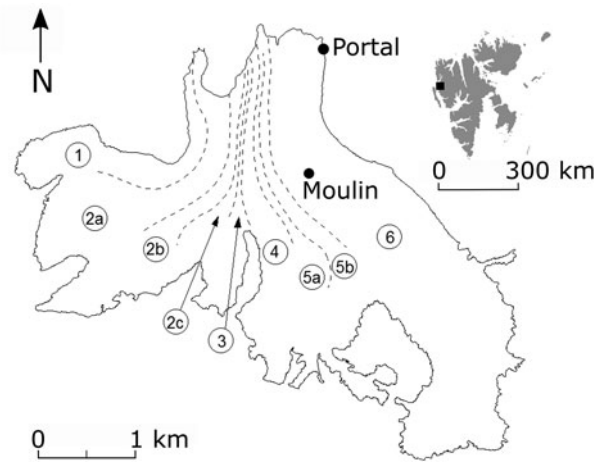

Fig. 1. Map of Austre Brøggerbreen. The moulin investigated with TLS is located ~1200 m from the glacier terminus. Numbered flow unit boundaries as identified by Jennings and others (2015), and the portal through which englacial drainage exits the glacier, are depicted. The location of Austre Brøggerbreen within Svalbard is highlighted on the inset map.

Since 1998, a persistent englacial conduit on the eastern-most flow unit has been repeatedly mapped using traditional cave surveying techniques, in order to characterise its morphological evolution. Over time, the channel has changed from an incised, down-glacier sloping supraglacial stream with many knickpoints, to a vertical moulin descending to a depth of ~50 m below the ice surface, which then feeds a low gradient, meandering englacial system (Myreng, 2015; Vatne and Irvine-Fynn, 2016).

2.2. Fundamentals of TLS

Numerous detailed reviews of TLS are available (e.g. Heritage and Large, 2009; Vosselman and Maas, 2010; Lemmens, 2011), and we provide a brief overview of the key terms used herein. TLS is an active remote-sensing technique that allows reconstruction of the surface of a feature in 3-D, using the emission and detection of a laser beam from a static point on the ground to calculate the distance between the object and the sensor (Pfiefer and Briese, 2007; Petrie and Toth, 2008; Heritage and Large, 2009). TLS typically uses an infrared wavelength laser beam that can be emitted either continuously (phase-shift method), or as a pulse (time-of-flight or pulse-based method (Petrie and Toth, 2008; Deems and others, 2013)). Each laser beam return creates a 3-D point in relative space around the instrument, producing a point cloud that represents the surface of a scanned object. The density and spacing of points is theoretically dependent on scan resolution, with optimal resolution being a trade-off between the highest number of points required for the project purpose and the scan duration. Resolution is an instrument parameter expressed as a fraction, with higher resolutions requiring greater scanning time. In the case of the FARO® Focus^{3D} X 330 scanner used herein, a maximum resolution of 1/1 takes 30.34 min to complete (LaserscanningEurope, 2015); typical scans using this instrument are carried out at 1/5 to 1/4 resolution, taking 5–10 min.

2.3. TLS field surveying

TLS of the glacier surface surrounding the moulin entrance, the moulin shaft and englacial conduit were carried out over 4 d in March 2016, when the channel was hydrologically inactive. Scans were conducted using a FARO® Focus^{3D} X 330 phase-shift scanner (360° horizontal field-of-view; 300° vertical field-of-view) with a shortwave infrared wavelength of 1550 nm (FARO Technologies Inc., 2013), mounted on a Gitzo™ Mountaineer carbon fibre tripod using a heavy duty 3/8″ camera fast-release mount. An insulation cover for the scanner head was fashioned from 0.8 cm

thick foam, with insertion of exothermic hand warmers at the base of the cover to prevent the scanner from becoming inoperable in sub-zero temperatures (Fig. 2). Three scans at 1/4 resolution (point spacing of 6.14 mm at a 10 m range (LaserscanningEurope, 2015)) were completed around the moulin circumference at the glacier surface, using the in-built GPS scanner function. In the absence of GPS signal below the ice, these surface scans provided georeferenced data from which the conduit point clouds were converted to absolute coordinates. Consequently, a higher resolution was used for the surface scans than that used for the conduit. Four spherical fishing buoys (radius: 10.4 cm) mounted on short drainpipe sections were used as targets, with their positions recorded using a portable Trimble Pathfinder® Pro XR differential GPS (dGPS), which were used to further correct surface scans to horizontal and vertical precisions of 0.61 and 1.68 m, respectively. Surface scans were conducted as close to the moulin entrance as safely possible, enabling scanning of the uppermost 3 m of the moulin shaft, relative to which the below-surface scans were co-registered.

Mapping of the uppermost englacial conduit reach was achieved by conducting 25 laser scans, extending from the base of the moulin to a horizontal distance along the thalweg of 122 m. Scans were carried out at 1/5 resolution (point spacing of 7.67 mm at a 10 m range (LaserscanningEurope, 2015)) and were acquired at horizontal intervals of between 1.75 and 9 m, with the TLS instrument mounted ~1.5 m above the cave floor. This variability in scan spacing depended on the channel sinuosity, with positioning to achieve maximum wall coverage using the minimum number of scans. Similarly, positioning of the scanner within the channel cross-section depended on the conduit morphology, in order to minimise beam shadowing. Double-sided 'A4' (29.7 × 21 cm) planar checkerboard targets were attached to ice screws using crocodile clips and inserted at varying heights perpendicular to the conduit walls, with smaller 'A5' (21 × 14.8 cm) targets of the same design placed at shorter spatial intervals at floor level (Fig. 2). These targets were positioned to ensure scan coverage of a minimum of three registration tie-points through forward planning of the subsequent two scanner locations, allowing for the likelihood of targets being knocked within the confined space. At each scan location, in situ air temperature and relative humidity were recorded using a Kestrel® 3000 pocket weather meter. Scan validation was accomplished through manual surveying of a 58 m conduit section, using a Leica Disto™ laser range finder and compass, to a survey grade 2/3 C (BCRA, 2017).

2.4. Point cloud processing

The resulting 3-D point clouds were post-processed using FARO® SCENE (FARO Technologies Ltd, 2016) and Rhino3D® (Robert McNeel & Associates, 2017) software. Surface scans were georeferenced and corrected using the dGPS coordinates of the spherical targets to enable below-surface scan registration in absolute coordinates. The conduit scans were relatively positioned, using the common moulin shaft sides and cornices captured in both the surface and below-surface scans. The depth and angular positioning of the conduit scans was corroborated by knowledge of the unloaded abseil rope length, and through examination of 360° photography of the moulin base (Digital Explorer, 2016). Manual registration of conduit scans enabled greater operator control, due to the lack of distinguishable features within the channel from which automatic algorithms could match overlapping areas. Registration of each scan to the preceding scan was conducted to within 6.8 mm positional accuracy, using between three and eight tie-points to achieve the lowest orthogonal mismatches possible.

Using FARO® SCENE, filtering of individual point clouds to remove speckle and edge effect noise was carried out

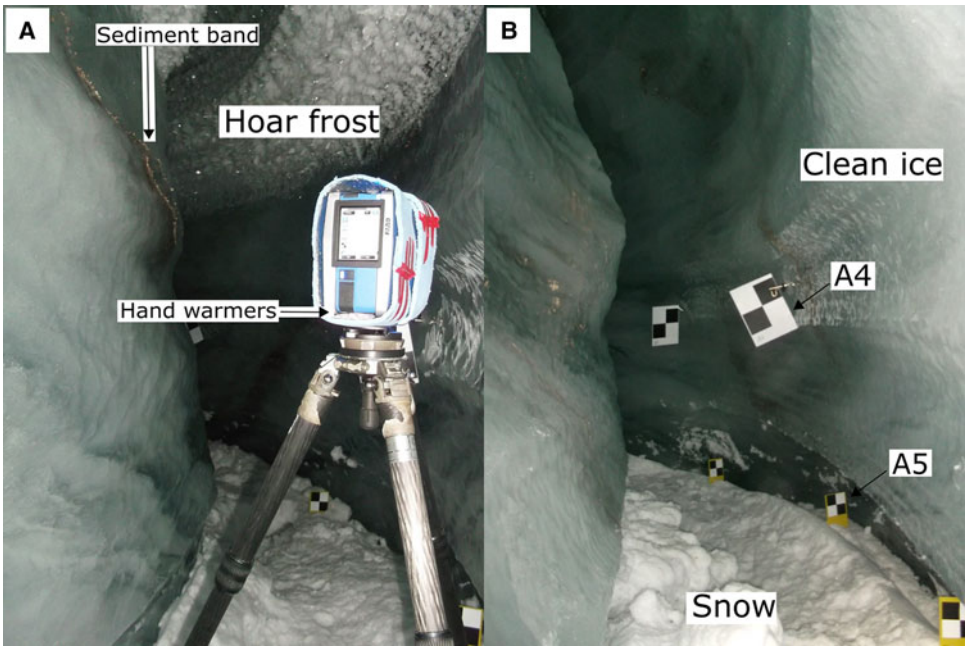

Fig. 2. The scanner in situ (A) demonstrating the insulation cover and placement of the exothermic hand warmers. Scalloping can be seen on the wall to the left of the scanner. Placement of the checkerboard targets within the conduit (B) on the wall and floor of the channel, with spacing of the latter at ⩾1 m. Longitudinal grooves are visible on the right wall. Both images show the snow, hoar frost, clean glacier ice and sediment-rich ice surfaces present within the channel.

post-registration to allow for retention of tie-points, with application of 'distance-based' and 'stray' filters removing 14.75 ± 5% of scan points. Filtering thresholds were established to remove visible noise, ensuring minimal compromising of the dataset, which would otherwise prevent mapping of cross-section morphology. Reflectivity percentages were calculated from the dimensionless raw reflectivity values of each point, in order to create a meaningful measure of reflectance from which to interpret the point cloud. Laser beam returns, defined as light reflected back to the scanner to create a point, are expressed as a percentage of the theoretical maximum number of laser returns.

2.5. Extraction of 2-D channel geometry

Digitisation of the filtered point clouds to extract 2-D geometry was completed using Rhino 3D® software with the Veesus Arena4D point cloud plugin, using point cloud slicing in the horizontal and vertical planes. Slicing widths were determined through visual inspection of the point cloud slices, to provide the best representation of a discrete profile while accounting for data losses. Linear representations of these point cloud slices were created by manually drawing lines of best fit through the centre of the points. Manual digitisation allowed for user control, accounting for areas of data exclusion and preventing incorrect mapping of edge effects. The channel planform was digitised at 1 m above the channel floor throughout the conduit. The moulin base was digitised 3 m above the floor, in order to exclude the snow and ice-block infill at the bottom of the shaft. Cross-section geometries were extracted using a 0.2 m width slice at 1 m intervals from the conduit entrance.

3. RESULTS

3.1. Englacial channel morphology

Throughout the conduit, the channel walls comprised clean glacier ice, with evidence of scalloping, tensional veins and continuous sediment bands of reddish-brown and light-grey colour cutting across the walls. Although numerous, these bands did not account for a large surface area. Hoar frost covered the uppermost sections of the conduit wall and ceiling, and snow composed of visibly large, consolidated crystals formed a blocky false floor (Fig. 2). Snow on the order of metres to several tens of metres thick unevenly covered the base of the moulin.

The 25 point clouds comprise over 261 million individual points, from which channel morphology was extracted (Fig. 3). Figure 3A shows that the conduit leads south-west from the base of the moulin, at a depth of 48 m below the ice surface. The channel planform shows regular meanders, with a high sinuosity of 2.7 and a curvature radius of 4 m. Over the mapped reach of 122 m, the channel lowers by 5.65 m, with a step made up of ice breccia covered by winter snowfall observed at the channel entrance accounting for 4.93 m of this (Fig. 3B). From the base of this step, the remainder of the channel remains relatively flat, lowering by only 0.67 m over 116 m length.

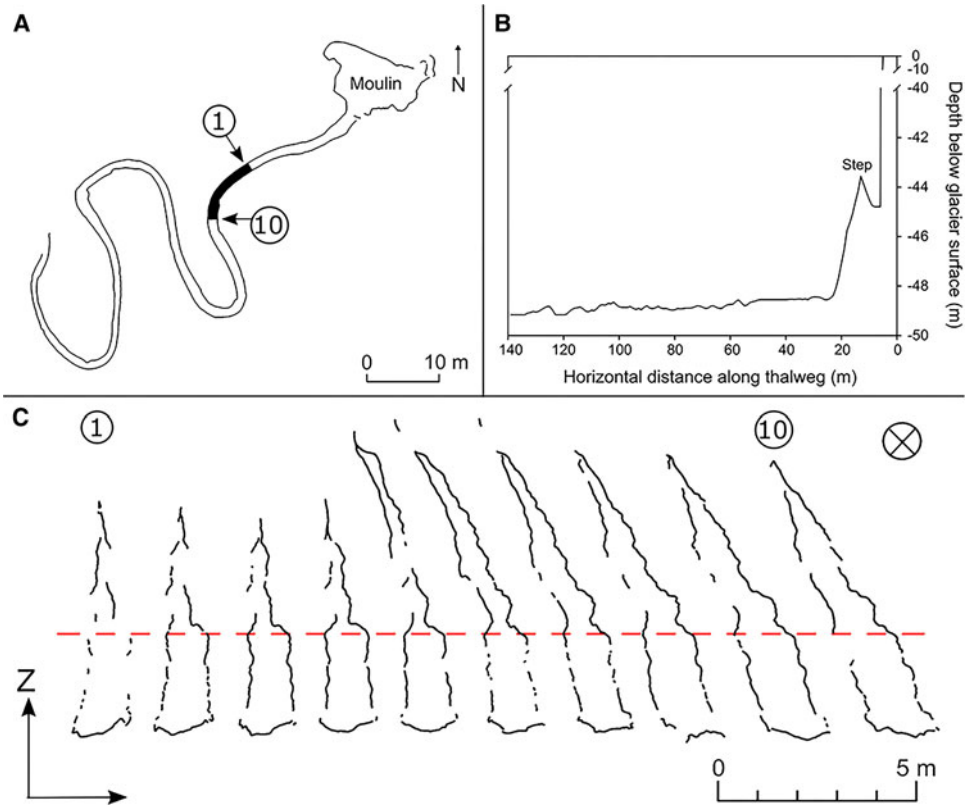

Fig. 3. (A): The channel planform, with the section used for cross-section analysis in (C) highlighted in black. The numbers correspond with those in (C) to denote cross-section locations; (B) the longitudinal profile – the dip at the base of the moulin shaft denotes the snow-covered moulin floor, with the rise in elevation to the top of the step; (C) channel cross-section morphology at 1 m intervals around the first meander bend blacked out in (A), progressing from left to right. The direction of flow is into the page, with the red dashed line providing a reference plane at 2 m above the floor. The teardrop shape with the presence of grooves and the tilt towards the inside bend can be seen. Discontinuous lines indicate areas without data, as a result of beam shadowing.

The conduit cross-section morphology is generally teardrop shaped, with tapering walls that meet between 5 and 12 m above the channel floor. Analysis of cross-section change with distance downstream demonstrates that the axis of the teardrop shape becomes increasingly tilted towards the inside bank around meander bend apexes, with a tilt of up to 25° being observed over a 10 m reach (Fig. 3C). Longitudinal grooves run the length of the conduit on either wall, with irregular groove spacing ranging between 0.94 and 2.05 m. The conduit width wall-to-wall is widest at the entrance to the channel (1.97 m), decreasing to <1 m downstream, with the narrowest section (0.68 m) located 6 m from the end of the mapped reach.

3.2. Conduit wall laser returns

Despite the point cloud successfully providing highly detailed 3-D visualisation of the conduit interior at a fine spatial resolution (Fig. 4), the overall laser returns were 38 ± 16%, indicating that nearly two-thirds of the emitted laser beams were not reflected back to the instrument. Several areas of each point cloud are devoid of data, most notably at regular vertical intervals along the channel wall and some sections of the conduit ceiling (Fig. 3C), resulting in 'holey' point clouds. The reflectivity percentage of the clean ice walls decreases significantly as the angle of incidence increases ($r = -0.47$, $n = 50$, $P \leqslant 0.01$): incidence angles of <30° exhibit a reflectivity of 31%, compared with 22–25% for angles >30°.

Analysis of reflectivity data indicates the presence of four reflectively distinct zones within the conduit. These differences are manifested spatially as contrasts between the channel floor, roof, and walls, with respective reflectivity percentages of 34 ± 4%, 31 ± 5% and 24 ± 5%, with thin linear features of 46 ± 7% reflectivity cutting across the conduit walls (Fig. 5). These variations correspond with snow cover at the base of the channel, hoar frost crystals in the conduit ceiling and the clean ice walls with entrained sediment bands, as validated from colour photographs taken at each scanner location. Results of analysis of variance tests indicate a significant difference between each of these surfaces ($P < 0.01$). Numerous thin bands of high reflectivity (40 ± 4%) were identified on the scans that were not immediately visible in the optical imagery (Fig. 5B), but through image analysis were found to be associated with sediment inclusions that were not exposed at the ice-wall surface. Similar to ice, a positive relationship between incidence angles and snow reflectivity was found ($r = 0.53$, $n = 50$, $P \leqslant 0.01$).

3.3. Accuracy and precision

The registration accuracy has a maximum error of 6.8 mm, with a mean error of 3.3 mm, representing the std dev. of orthogonal registration mismatch between adjacent scans, expressed as cumulative distance offset in the X, Y and Z planes (FARO Technologies Inc., 2015). However, the unclosed traverse from the moulin base to the end of the scanned conduit prevents equal error distribution between scans. This yields a maximum combined absolute error of 73 mm by the end of the traverse, derived from the sum of orthogonal mismatches for the 25 scans.

In order to evaluate the accuracy at which the laser beam identifies the solid ice surface, variance of the point cloud data from a plane of best fit was quantified (linear least squares; $n = 50$). Although flat 0.05 m^2 areas of the conduit wall devoid of sediment inclusions were selected for this analysis, it must be acknowledged that the ice surface is

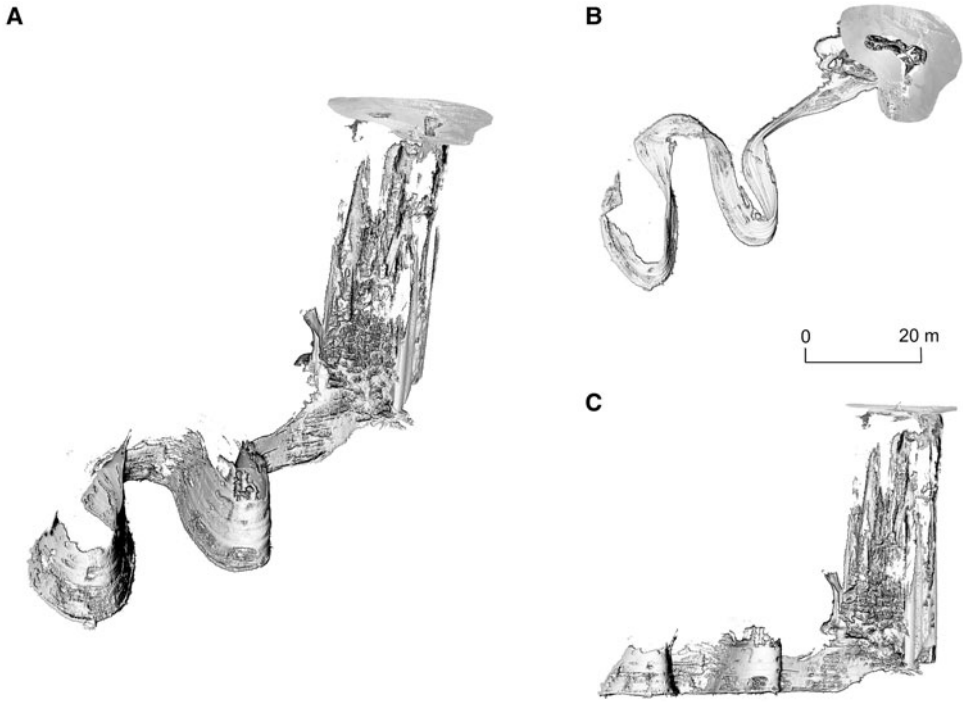

Fig. 4. Three-dimensional point cloud visualisation of the moulin shaft and englacial conduit, showing perspective (A), plan (B) and side (C) views to demonstrate the success of the TLS reconstruction. For further visualisation of the TLS survey results in three-dimensions, the reader is directed to the following links for a fly-through video of the moulin and conduit (www.youtube.com/watch?v=o7uOGKb0kwc) and panoramic visualisation of the interior (www.derij.co.uk/images/panos/SV2016/SV2016.html).

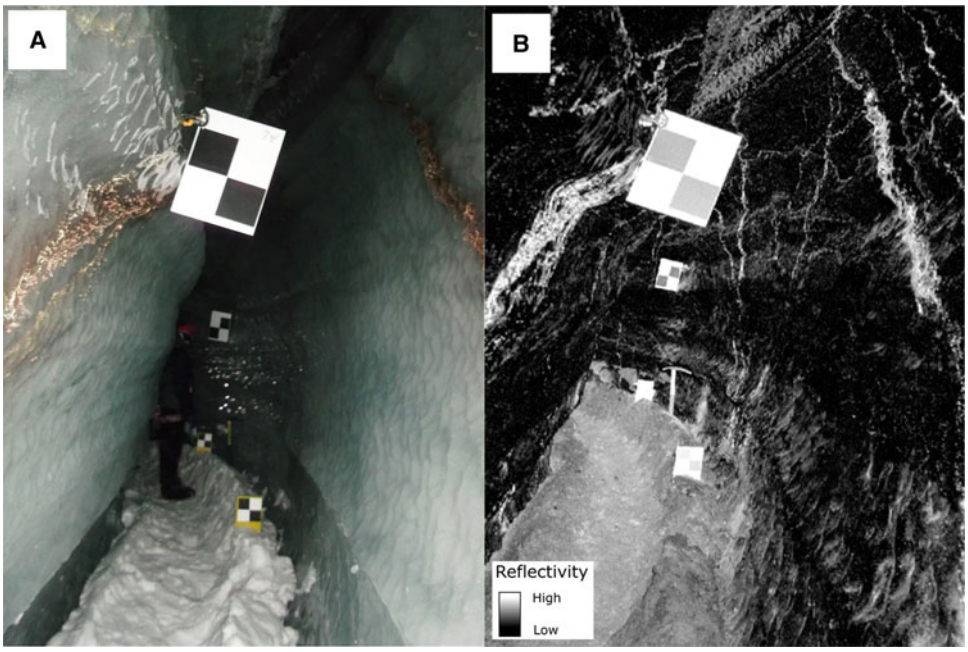

Fig. 5. Colour photograph (A) and greyscale visualisation of scan reflectivity values for the same view (B), demonstrating differences in laser beam return from varying materials. Visible sediment bands cutting across either conduit wall can be seen in both panels, with fine vertical stripes visible on the right wall of (B) showing the thinner sediment bands or fractures that are not exposed at the ice wall; hoar frost can be seen on the upper section of this wall. Wall targets (A4) and floor targets (A5) are visible in both image panels for scale. Additional scale visible just left-of-centre includes a person (panel A) and an ice axe (panel B).

inevitably curved over an area containing sufficient points to enable plane fitting. This method yields an accuracy of ±6.54 mm for detection of the ice walls, compared with a mean error of ±2.19 mm for the solid surface of the checkerboard targets (comparable to the quoted manufacturer's accuracy of ±2 mm (FARO Technologies Inc., 2011)).

Despite the scatter of points around the plane of best fit being within 1 cm of the ice wall surface, the scans reveal numerous individual points located at apparently regular intervals beyond the channel wall (⩽0.61 m). These extraneous points are arranged as a series of linear features parallel to the channel walls, and correspond with the location of the ice screws holding the checkerboard targets in place (Fig. 6). These features are interpreted to be representative of ice fracturing, which occurred perpendicularly around the shaft of the screw during insertion (e.g. Hill, 2006).

Assessment of scan precision was achieved through quantification of linear offsets between areas of overlapping scans ($n = 50$). Planes of best fit were created for areas of point cloud overlap between adjacent scans, with measurement of each individual scan's point cloud deviation from this plane. This provided an overall scan precision of ±10 cm.

3.4. Influence of meteorological conditions

Within the conduit, air temperature varied between −1 and −4.9°C, typically being ∼−3.5°C. Relative humidity was between 79 and 97%, compared with an average March atmospheric relative humidity of ∼70% for the nearby settlement of Ny-Ålesund at 2 m above ground (Maturilli and others, 2013). The FARO® Focus^{3D} X 330 provided consistent instrumental operation in temperatures as low as −5°C, providing that the scanner temperature remained above 3°C. Insulation of the scanner head maintained instrument temperatures of >17°C throughout the duration of surveying, with air temperature having a negligible effect. However, ceasing of instrument operation for 50 min resulted in a decrease in scanner temperature from 21 to 3°C, with recommencement leading to a temperature rise of 14°C in 20 min, as a result of the scanner generating heat when operating. Although correlations between meteorological conditions and laser beam returns show that higher returns are associated with colder temperatures and lower relative humidity (respectively, $r = -0.47$; $r = 0.2$, $n = 17$), these relationships are not significant ($P > 0.05$). However, wind chill at the glacier surface lowered air temperatures to −25°C, resulting in scanner shutdown. Cold operating temperatures also slowed the rate at which scan surveys could be conducted, as a result of the logistical impacts of undertaking fieldwork in low-temperature environments.

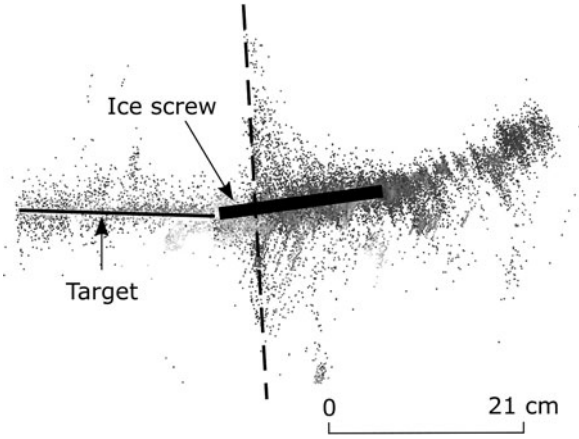

Fig. 6. Plan view of the A4 checkerboard target and the points within the channel wall, interpreted as fracturing of the ice around the ice screw shaft during insertion. The dotted line denotes the ice wall surface. Points surrounding the target are the result of edge effect noise that is visible when presented in plan view.

4. INTERPRETATION AND DISCUSSION

4.1. Channel morphology

The englacial channel's longitudinal profile and planform are consistent with the previous conduit survey conducted in 2014, which demonstrated regular meandering at a constant depth (Myreng, 2015). The development of the vertical moulin shaft and these meanders were first recorded in 2008 (Vatne and Irvine-Fynn, 2016), indicating that these features may be relatively stable in their general form over annual to inter-annual timescales. As changes in channel bed slope are one of the most efficient ways of dissipating energy (Knighton, 1998), the consistent conduit depth indicates that adequate energy dissipation is achieved by the existing channel morphology. This suggests that the vertical drop of water over the moulin edge acts to efficiently dissipate the majority of the stream's energy (Curran and Wohl, 2003).

The teardrop cross-section morphology denotes passage closure as a result of ice creep deformation, bringing the two walls into contact to form a sutured canyon indicative of the channel's cut-and-closure origin (Gulley and others, 2009a). Furthermore, the longitudinal grooves are interpreted to represent fluctuations in, or modes of, meltwater discharge (Vatne and Irvine-Fynn, 2016), with lateral thermal expansion at times of high discharge and vertical channel incision under reduced flow conditions (Marston, 1983).

4.2. Laser returns from clean ice

In the fully enclosed conduit environment, the low percentage of overall returns is likely explained by the properties of the scan surface or the environmental conditions (Smith, 2015). The majority of the scanned surface comprised clean ice, which has a high absorption coefficient in the infrared (~1.6 cm^{-1}) with significant absorption bands around the 1550 nm wavelength of the scanner used herein (Hobbs, 1974; Warren and Wiscombe, 1981; Warren, 1982). The depth to which electromagnetic radiation can penetrate below the surface of a material is one of the primary variables controlling its reflectance (Picard and others, 2016), meaning that clear ice effectively absorbs these wavelengths (Hobbs, 1974; Lucey and Clark, 1985). This causes photon extinction just below the ice surface, accounting for laser beam losses and low returns. Such losses using infrared wavelengths have also been reported on glacier surface ice, where clean ice exhibited a low percentage of returns and, consequently, sparse data coverage (Hopkinson, 2004). Furthermore, the low reflectivity of the smooth, shiny, ice surface at high incidence angles causes laser beam deflection away from the scanner (Jörg and others, 2006; Soudarissanane, 2016), meaning that low amounts of radiation are reflected back to the instrument, resulting in reduced or no measurements (Heritage and Large, 2009). Therefore, distance from the scanner becomes a major limiting factor in scanning oblique ice surfaces, as the incidence angle increases with distance (Soudarissanane and others, 2008; Heritage and Large, 2009; Pejić, 2013).

The geometric properties of the conduit's ice wall can also influence the existence, location and intensity of a returned laser beam point (Lichti and others, 2002). The cross-section geometries show that the existence of a point is primarily dependent on the line-of-sight principle, with areas devoid of data coinciding with curved areas of the channel roof and the troughs of longitudinal grooves (Fig. 3C). This indicates laser beam obstruction, resulting in the creation of shadowed areas and, thus, determining the scan features that can be represented within the point cloud. Furthermore, the wall morphology underpins the intensity of the return, with ice surfaces perpendicular to the scanner providing the greatest intensities. This demonstrates that positioning of the scanner in relation to the conduit geometry determines the areas where beam reflectance will be maximised and, subsequently, point cloud density (Soudarissanane and others, 2011).

As the cool conditions within the englacial channel are considered favourable for laser scanning (Baltsavias, 1999), it would be expected that returns would be maximised in this environment. However, as Section 3.4 demonstrates no significant relationship between either air temperature or relative humidity and percentage returns, factors beyond the meteorological conditions reported here exert an influence on laser returns. This assertion is supported by the ability to achieve the instrument's reported accuracy of 2 mm on the target surfaces. Therefore, over these temperature and humidity ranges, the physical and optical properties of the conduit walls and glacier ice have a greater influence on the quality of laser returns in this environment.

4.3. Laser returns from snow, hoar frost and sediment

In the shortwave infrared, the laser returns from snow, hoar frost and sediment are significantly higher than that of the least reflective clean glacier ice herein, with reflectivity values at least 7% greater than the conduit walls. Although the spectral reflectance of snow and hoar frost is low in this wavelength (Foster and others, 1987; ESA, 2014), their absorption coefficients are lower than that of ice, meaning that they are more reflective (Joseph, 2005), with the higher surface roughness of these materials further increasing their reflectivity (Choudhury and Chang, 1981; Schaffhauser and others, 2008). However, the greatest reflectivity is from the sediment bands, indicating the presence of high particle concentrations exposed at the wall surface and in the near-surface ice (Alfoldi, 1982; Lucey and Clark, 1985; Karabulut and Ceylan, 2005).

As the scan data detected thinner, discrete sediment bands that were not exposed at the wall surface, this suggests that the laser is able to detect sediment located at depths greater than the ice absorption coefficient. This could be the result of the sediment mineral properties, as the constituent minerals of the red sandstone, limestone and quartz bedrock geology underlying the eastern parts of Austre Brøggerbreen (Nowak and Hodson, 2014) have very high reflectance in the infrared, contributing to their detection within the ice substrate (Gibson, 2000; Choudhury and others, 2009). Although the sediment type within such discrete bands cannot be confirmed, the colour of the exposed sediment accords with this bedrock geology. Conversely, this detection may be facilitated by the evidence of below-surface ice fracturing (Fig. 6), which suggests that the laser may either: (i) be reflected from sub-surface structural inhomogeneities, providing a return where homogeneous intact ice does not, and/or (ii) be able to exploit existing structural weaknesses when scanned at certain angles.

4.4. Data quality and methodological considerations

The accuracy assessment demonstrates that TLS can provide high-quality data, accurate at millimetre scale. As the errors

seen here for ice surface detection are three times greater than the quoted manufacturer's accuracy, it is reasonable to surmise that this discrepancy is the result of the scanned surface properties (Section 4.2), influencing point distribution and density which ultimately determines spatial accuracy (Höfle and others, 2007; Tedesco, 2015). This is a notable improvement on previous surveys of ice-walled channels, which typically provide centimetre-scale error (Vatne and Refsnes, 2003; Müller, 2007; Gulley and others, 2009a,b; Naegeli and others, 2014). The ability of TLS to yield sub-centimetre measurements demonstrates the potential for investigation of morphological change over shorter timescales than have been previously achievable. As the rate of change observed in supraglacial channels feeding into englacial conduits is on the order of centimetres per day (Gulley and others, 2009a), traditional surveying is, therefore, limited to identifying change occurring over several months to a year at best, discounting the fact that some englacial channels may only change at a rate of centimetres per year.

The scatter of points recorded around the accuracy assessment plane of best fit is thought to indicate laser beam penetration of the clear ice surface, demonstrating the short photon path length in a material with a high absorption coefficient (Kargel and others, 2014). This shows that the depth of penetration for intact ice is small, supporting measurements conducted by Asner and Ollinger (2009), which ranged from a few millimetres to tens of centimetres for glacier ice. Although the error in detection of the channel walls inevitably influences point cloud precision, introducing additional offset between overlapping scan sections, Section 4.2 demonstrated that the existence and location of an individual point is dependent on the scan geometry and positioning of the TLS instrument relative to the scanned surface. Therefore, the likelihood of obtaining points from adjacent scans that are close to one another in 3-D space is further reduced (Pfiefer and Briese, 2007; Smith, 2015). However, it is not uncommon for actual point precision to be lower than values quoted by the manufacturer, as there are several environmental variables that can degrade this figure such as the surface properties and angle of laser beam incidence, and error introduction in the point cloud processing stages (Buckley and others, 2008), as demonstrated herein.

Clearly, the challenging nature of the englacial environment and associated variable reflectance properties of the conduit reduce data quality. In theory, certain techniques could be used to reduce ice wall reflectance and provide improved laser returns, such as scraping of the surface to increase roughness or covering the walls with calibrated Spectralon coating (Soudarissanane, 2016). However, such interventions would be both impractical and time-consuming, and would not describe the true geometry or allow distinction of differing surface types.

It must be acknowledged that the use of infrared wavelengths, which are readily absorbed by water, also contribute to the low percentage of laser returns and, thus, influences point cloud coverage. However, although green-wavelength systems may provide better return signals due to being absorbed less by water, these systems are not necessarily more appropriate for this application. Infrared TLS systems use phase-shift technology, which is not only more suited for scanning at short ranges (Gallay and others, 2015), such as within englacial conduits, but affords faster measurements and increased precision over green-wavelength pulse-based technology (Pfiefer and Briese, 2007; Smith, 2015; Soudarissanane, 2016). Furthermore, the FARO® Focus^{3D} X 330 was selected over other TLS instruments for its practicality within the glacial environment, in that it provides a robust and lightweight, compact instrument (5.2 kg without battery) that has both the speed and internal power necessary for mapping englacial conduits.

4.5. Advantages and potential of TLS in glacio-speleology

Experience from this project demonstrates that TLS provides several advantages for mapping of englacial conduit morphology over traditional cave surveying techniques. Firstly, the fine TLS spatial resolution affords a more detailed insight into smaller-scale morphological features, particularly with respect to channel cross-sections, where traditional surveys tend to identify overall shape and are subject to human perception (e.g. Judson, 1974). Secondly, the time frame for acquisition of such high-resolution data is remarkably shortened when compared with that required to obtain equivalent measurement detail using traditional surveying techniques. Despite producing large, storage-heavy point clouds (Petrie and Toth, 2008), analysis of TLS data is increasingly easy to undertake, with several free, open-source, software packages now being available, such as CloudCompare (CloudCompare, 2004) and MeshLab (MeshLab, 2008). Although a TLS system can be expensive, the price of commercial laser scanners has reduced significantly over the last decade (Wehr, 2008) and continues to fall. These advantages clearly facilitate opportunities to readily retrieve comparative 'snapshots' of the englacial drainage system from which to better identify the nature and rate of conduit morphology change, as has been demonstrated in terrestrial rivers (Resop and Hession, 2010). The results described here highlight how TLS data may provide indications of the interaction between morphology and flow dynamics, and has the potential to provide datasets from which to validate predictive models of hydrological evolution (e.g. Jarosch and Gudmundsson, 2012). Through fully describing englacial hydrological systems at high resolution, it will be possible to explore and advance current understanding of processes operating in poorly characterised hydrological systems.

5. CONCLUSIONS

This study has demonstrated the novel use of TLS within an englacial conduit in a High Arctic, predominantly cold-based glacier. The key findings presented here are:

- TLS is a viable method for 3-D reconstruction of ice-walled channels, enabling retrospective millimetre-to-centimetre scale, 2-D mapping of conduit morphology, and extraction of geometric measurements at fine spatial resolutions. This has facilitated the first high-resolution, detailed insight of the cross-section geometry of an englacial channel, revealing teardrop shape morphology with irregularly spaced longitudinal grooves.
- Point cloud quality depends on the physical and optical properties of the surfaces within the conduit, herein comprising ice, snow, hoar frost and sediment, with their respective absorption coefficients in the shortwave infrared, reflectance type, and the complex conduit morphology determining point density and distribution. As a

result, laser returns within the englacial environment are low, typically <50%.
- The ice wall is not detected as a solid surface, with point accuracy of 6.54 mm. Although laser beam penetration into the uppermost ice layers is small, structural weaknesses allow penetration to, and reflection from, depths of ⩽0.6 m.
- The scanner used herein (FARO® Focus^{3D} X 330) operated at ambient air temperatures as low as −25°C, when insulated. Although extreme temperature conditions did not impact upon scan quality, they did influence survey efficiency.

In light of these conclusions, the following recommendations are proposed in order to obtain the highest quality results when surveying ice-walled channels:

(1) Precautions should be taken to prevent the scanner becoming too cold during transit and operation, with continual scanning once surveying has commenced to safeguard against instrument malfunction.
(2) Survey locations should be closely spaced, with scans every few metres to maximise returns at low incidence angles and afford sufficient overlap between adjacent point clouds. Numerous targets should be used to enable high registration accuracy, particularly due to the possibility of targets being knocked by investigators in the confined space.
(3) Englacial scanning can be efficiently conducted with a minimum of two investigators, with a third to assist in target setting helping to speed up the surveying process.

In conclusion, TLS is a robust method for high-resolution englacial conduit mapping, providing high-quality data that greatly improve upon the accuracy and detail of morphological analysis currently achieved by traditional cave surveying. The success of this innovative technique within glacio-speleology demonstrates the potential to reveal subsurface structural fractures, identify sedimentary features and obtain sequential surveys from which to quantify morphological change and network evolution. Application of this method in englacial and, where accessible, subglacial drainage mapping offers a powerful additional tool to yield data that will likely provide a useful input for water flux modelling, and contribute towards an enhanced process-level understanding of hydrological evolution.

ACKNOWLEDGEMENTS

This research is part-funded by the European Social Fund (ESF) through the European Union's Convergence programme (West Wales and the Valleys) administered by the Welsh government: Knowledge Economy Skills Scholarship (KESS) Project AU10003 awarded to TDLI-F and JEK, with support from Deri Jones & Associates Ltd. All authors recognise additional support from Aberystwyth University (DGES). Geir Vatne is thanked for insights relating to the englacial cave and for support with project inception. FARO is gratefully acknowledged for the loan of the scanner and restoration of scan metadata. Support from the UK NERC Arctic Research Station, and Kings Bay AS and associated personnel including Nick Cox was gratefully received. Blair Fyffe, James Wake and Paula O'Sullivan of BAS are thanked for on-site assistance and support in the field. Sille Myreng kindly provided accurate GPS coordinates for the moulin entrance; and helpful comments and insights were gratefully received from Ian Stevens and Emily Parker. The authors thank Rob Bingham and an anonymous reviewer for their comments, which helped improve the manuscript. Data are available on request.

AUTHOR CONTRIBUTIONS

TDLI-F conceived the project idea and designed the research; JEK, JPPJ and SJAJ conducted the research; JEK processed and analysed the data with assistance from JPPJ and PB. JEK wrote the manuscript and all authors edited and revised the paper.

REFERENCES

Alfoldi TT (1982) Remote sensing for water quality monitoring. In Johannsen CJ and Sanders JL eds. *Remote sensing for resource management*. Soil Conservation Society of America, Ankey, Iowa, 317–328

Asner GP and Ollinger SV (2009) Remote sensing for terrestrial biogeochemical modeling. In Warner TA, Nellis MD and Foody GM eds. *The SAGE handbook of remote sensing*. SAGE Publications Ltd., London, 411–422

Bælum K and Benn DI (2011) Thermal structure and drainage system of a small valley glacier (Tellbreen, Svalbard), investigated by ground penetrating radar. *Cryosphere*, **5**(1), 139–149 (doi: 10.5194/tc-5-139-2011)

Baltsavias EP (1999) Airborne laser scanning: basic relations and formulas. *Int. Soc. Photogramme*, **54**, 199–214 (doi: 10.1016/S0924-2716(99)00015-5)

Barrand NE, James TD and Murray T (2010) Spatio-temporal variability in elevation changes of two high-Arctic valley glaciers. *J. Glaciol.*, **56**(199), 771–780 (doi: 10.3189/002214310794457362)

BCRA (British Cave Research Association) (2017) BCRA survey grades, BCRA, 03/07/2017 [web page]. http://www.cavinguk.co.uk/info/Surveygrade.htm

Benn DI, Gulley JD, Luckman A, Adamek A and Glowacki PS (2009) Englacial drainage systems formed by hydrologically driven crevasse propagation. *J. Glaciol.*, **55**(191), 513–523 (doi: 10.3189/002214309788816669)

Bingham RG, Nienow P, Sharp M and Boon S (2005) Subglacial drainage processes at a high Arctic polythermal valley glacier. *J. Glaciol.*, **51**(172), 15–24 (doi: 10.3189/172756505781829520)

Björnsson H and 6 others (1996) The thermal regime of sub-polar glaciers mapped by multi-frequency radio-echo sounding. *J. Glaciol*, **42**(140), 23–32 (doi: 10.1017/s0022143000030495)

Bruland O and Hagen JO (2002) Glacial mass balance of Austre Brøggerbreen (Spitsbergen), 1971-1999, modelled with a precipitation-run-off model. *Polar Res.*, **21**(1), 109–121 (doi: 10.1111/j.1751-8369.2002.tb00070.x)

Buchroithner MF, Gaisecker D, Gaisecker T and Österreich H (2009) Terrestrial laser scanning for the visualization of a complex dome in an extreme Alpine cave system. *Photogramm. Fernerkun*, **4**, 329–339 (doi: 10.1127/1432-8364/2009/0025)

Buckley SJ, Howell JA, Enge HD and Kurz TH (2008) Terrestrial laser scanning in geology: data acquisition, processing and accuracy considerations. *J. Geol. Soc. London*, **165**, 625–638 (doi: 10.1144/0016-76492007-100)

Catania GA, Neumann TA and Price SF (2008) Characterizing englacial drainage in the ablation zone of the Greenland ice sheet. *J. Glaciol.*, **54**(187), 567–578 (doi: 10.3189/002214308786570854)

Choudhury BJ and Chang ATC (1981) The albedo of snow for partially cloudy skies. *Bound.-Layer Meteorol.*, **20**, 371–389 (doi: 10.1007/BF00121380)

Choudhury S, Chakrabarti D and Choudhury S (2009) *An introduction to geographic information technology*. I.K. International Publishing House Pvt. Ltd., New Delhi

CloudCompare (2004) *3D point cloud and mesh processing software*, Girardeau-Montaut, D., Open Source Project

Cosso T, Ferrando I and Orlando A (2014) Surveying and mapping a cave using 3d laser scanner: the open challenge with free and open source software. *Int. Soc. Photogramme*, **XL-5**, 181–186 (doi: 10.5194/isprsarchives-XL-5-181-2014)

Curran JH and Wohl EE (2003) Large woody debris and flow resistance in step-pool channels, Cascade Range, Washington. *Geomorphology*, **51**(1–3), 141–157 (doi: 10.1016/s0169-555x(02)00333-1)

Das SB and 6 others (2008) Fracture propagation to the base of the Greenland Ice sheet during supraglacial lake drainage. *Science*, **320**, 778–781 (doi: 10.1126/science.1153360)

Deems JS, Painter TH and Finnegan DC (2013) Lidar measurement of snow depth: a review. *J. Glaciol.*, **59**(215), 467–479 (doi: 10.3189/2013JoG12J154)

Digital Explorer (2016) Google Street View - Ny- Ålesund, March 2016, Google Maps, 03/07/2017 [web page]

ESA (European Space Agency) (2014) Optical properties of ice and snow, ESA, 03/07/2017 [web page]. https://www.esa.int/SPECIALS/Eduspace_Global_EN/SEMPJ7TWLUG_0.html#subhead1

FARO Technologies Inc. (2011) *FARO laser scanner Focus3D manual*. FARO Technologies Inc., Barcelona

FARO Technologies Inc. (2013) *FARO laser scanner Focus3D X 330 features, benefits and technical specifications*. FARO Technologies Inc., Barcelona

FARO Technologies Inc. (2015) *SCENE 5.5.3 user manual*. FARO Technologies Inc., Barcelona

FARO Technologies Ltd. (2016) *SCENE, 5.5.3 software*. FARO Technologies Ltd., Warwickshire

Fischer M, Huss M, Kummert M and Hoelzle M (2016) Application and validation of long-range terrestrial laser scanning to monitor the mass balance of very small glaciers in the Swiss Alps. *Cryosphere*, **10**(3), 1279–1295 (doi: 10.5194/tc-10-1279-2016)

Foster JL, Hall DK and Chang ATC (1987) Remote sensing of snow. *Eos, Trans. Am. Geophys. Union*, **68**(32), 682–684 (doi: 10.1029/EO068i032p00682-01)

Fountain AG and Walder JS (1998) Water flow through temperate glaciers. *Rev. Geophys.*, **36**(3), 299–328 (doi: 10.1029/97rg03579)

Fountain AG, Jacobel RW, Schlichting R and Jansson P (2005) Fractures as the main pathways of water flow in temperate glaciers. *Nature*, **433**, 618–621 (doi: 10.1038/nature03296)

Gabbud C, Micheletti N and Lane SN (2015) Lidar measurement of surface melt for a temperate Alpine glacier at the seasonal and hourly scales. *J. Glaciol.*, **61**(229), 963–974 (doi: 10.3189/2015JoG14J226)

Gallay M, Kaňuk J, Hochmuth Z, Meneely J and Hofierka J (2015) Large-scale and high-resolution 3-D cave mapping by terrestrial laser scanning: a case study of the Domica Cave, Slovakia. *Int. J. Speleol.*, **44**(3), 277–291 (doi: 10.5038/1827-806x.44.3.6)

Gibson PJ (2000) *Introductory remote sensing principles and concepts*. Routledge, Oxon

Gulley J (2009) Structural control of englacial conduits in the temperate Matanuska Glacier, Alaska, USA. *J. Glaciol.*, **55**(192), 681–690 (doi: 10.3189/002214309789470860)

Gulley JD, Benn DI, Müller D and Luckman A (2009a) A cut-and-closure origin for englacial conduits in uncrevassed regions of polythermal glaciers. *J. Glaciol.*, **55**(189), 66–80 (doi: 10.3189/002214309788608930)

Gulley JD, Benn DI, Screaton E and Martin J (2009b) Mechanisms of englacial conduit formation and their implications for subglacial recharge. *Quat. Sci. Rev.*, **28**(19–20), 1984–1999 (doi: 10.1016/j.quascirev.2009.04.002)

Hagen JO and Sætrang A (1991) Radio-echo soundings of sub-polar glaciers with low-frequency radar. *Polar Res.*, **9**(1), 99–107 (doi: 10.3402/polar.v9i1.6782)

Hagen JO, LiestøL O, Erik R and Jørgensen T (1993) *Glacier atlas of Svalbard and Jan Mayen*. Norsk Polarinstitutt, Oslo

Harper JT and Humphrey NF (1995) Borehole video analysis of a temperate glacier's englacial and subglacial structure: implications for glacier flow models. *Geology*, **23**(10), 901–904 (doi: 10.1130/0091-7613(1995)023<0901:BVAOAT>2.3.CO;2)

Heritage GL and Large ARG (2009) *Laser scanning for the environmental sciences*. Wiley-Blackwell, Chichester

Hill P (2006) *International handbook of technical mountaineering*. David & Charles Ltd., Cincinnati

Hobbs PV (1974) *Ice physics*. Oxford University Press, Oxford

Höfle B, Geist T, Rutzinger M and Pfiefer N (2007) Glacier surface segmentation using airborne laser scanning point cloud and intensity data. In *International Archives of the Photogrammetry, Remote Sensing and Spatial Information Sciences*, Espoo, Finland, 36(3), 195–200

Holmlund P (1988) Internal geometry and evolution of moulins, Storglaciären, Sweden. *J. Glaciol.*, **34**(117), 242–248 (doi: 10.1017/S0022143000032305)

Hopkinson C (2004) *Place glacier terrain modeling and 3D laser imaging*. Otterburn Geographic and Applied Geomatics Research Group, Nova Scotia

Idrees MO and Pradhan B (2016) A decade of modern cave surveying with terrestrial laser scanning: a review of sensors, method and application development. *Int. J. Speleol.*, **45**(1), 71–88 (doi: 10.5038/1827-806x.45.1.1923)

Iken A and Bindschadler RA (1986) Combined measurements of subglacial water pressure and surface velocity of Findelengletscher, Switzerland: conclusions about drainage system and sliding mechanism. *J. Glaciol.*, **32**(110), 101–119 (doi: 10.1017/S0022143000006936)

Irvine-Fynn TDL, Hodson AJ, Kohler J, Porter PR and Vatne G (2005) Dye tracing experiments at Midre Lovénbreen, Svalbard: preliminary results and interpretations. 7th GLACKIPR Conference, Moscow, Russia, 36–43

Irvine-Fynn TDL, Hodson AJ, Moorman BJ, Vatne G and Hubbard AL (2011) Polythermal glacier hydrology: a review. *Rev. Geophys.*, **49**(4), 1–37 (doi: 10.1029/2010rg000350)

Jansson P, Hock R and Schneider T (2003) The concept of glacier storage: a review. *J. Hydrol.*, **282**(1–4), 116–129 (doi: 10.1016/s0022-1694(03)00258-0)

Jarosch AH and Gudmundsson MT (2012) A numerical model for meltwater channel evolution in glaciers. *Cryosphere*, **6**(2), 493–503 (doi: 10.5194/tc-6-493-2012)

Jennings SJA, Hambrey MJ, Glasser NF, James TD and Hubbard B (2015) Structural glaciology of Austre Brøggerbreen, northwest Svalbard. *J. Maps*, **12**(5), 790–796 (doi: 10.1080/17445647.2015.1076744)

Jörg P, Fromm R, Sailer R and Schaffhauser A (2006) Measuring snow depth with a terrestrial laser ranging system. In *Proceedings of the 2006 International Snow Science Workshop*, Telluride, Colorado, 452–460

Joseph G (2005) *Fundamentals of remote sensing*. 2nd edn. Universities Press (India) Private Limited, Hyderabad

Judson D (1974) Cave surveying for expeditions. *Geogr. J.* **140**(2), 292–300 (doi: 10.2307/1797087)

Kaasalainen S, Kaartinen H and Kukko A (2008) Snow cover change detection with laser scanning range and brightness measurements. *EARSeL eProc.*, **7**, 133–141

Karabulut M and Ceylan N (2005) The spectral reflectance responses of water with different levels of suspended sediment in the presence of algae. *Turkish J. Eng. Environ. Sci.*, **29**, 351–360

Kargel JS, Leonard GJ, Bishop MP, Kääb A and Bruce H (2014) *Global land ice measurements from space*. Springer-Verlag Berlin Heidelberg, Berlin

Knighton AD (1998) *Fluvial forms and processes*. Hodder Arnold, London

Laserscanning Europe GmbH (2015) Correct resolution for laser scanning, Laserscanning Europe GmbH, 22/09/2017 [web page]. http://www.laserscanning-europe.com/en/news/correct-resolution-laser-scanning

Lemmens M (2011) Terrestrial laser scanning. *Geo-information: technologies, applications and the environment*. Springer, The Netherlands, Dordrecht, 101–121

Li J, Youchan W and Xianjun G (2012) A new approach for subway tunnel deformation monitoring: high-resolution terrestrial laser scanning. *XXII ISPRS Congress*, Melbourne, Australia, International Archives of the Photogrammetry, Remote Sensing and Spatial Information Sciences, 223–228

Lichti DD, Gordon SJ and Stewart MP (2002) Ground-based laser scanners: operation, systems and applications. *Geomatica*, **56** (1), 21–33

Lingle CS and Fatland DR (2003) Does englacial water storage drive temperate glacier surges? *Ann. Glaciol.*, **36**(1), 14–20 (doi: 10.3189/172756403781816464)

Lucey PG and Clark RN (1985) Spectral properties of water ice and contaminants. In Klinger J, Benest D, Dollfus A and Smoluchowski R eds. *Ices in the solar system*. Springer, The Netherlands, Dordrecht, 155–168

Mair D (2005) Thirty-seven year mass balance of Devon Ice Cap, Nunavut, Canada, determined by shallow ice coring and melt modeling. *J. Geophys. Res.*, **110**(F1), 1–13 (doi: 10.1029/2003jf000099)

Mankoff KD and Tulaczyk SM (2017) The past, present, and future viscous heat dissipation available for Greenland subglacial conduit formation. *Cryosphere*, **11**(1), 303–317 (doi: 10.5194/tc-11-303-2017)

Marston RA (1983) Supraglacial stream dynamics on the Juneau Icefield. *Ann. Assoc. Am. Geogr.*, **73**(4), 597–608 (doi: 10.1111/j.1467-8306.1983.tb01861.x)

Maturilli M, Herber A and König-Langlo G (2013) Climatology and time series of surface meteorology in Ny-Ålesund, Svalbard. *Earth Syst. Sci. Data*, **5**(1), 155–163 (doi: 10.5194/essd-5-155-2013)

MeshLab (2008) *MeshLab: an Open-Source Mesh Processing Tool*, Sixth Eurographics Italian Chapter Conference, 129–136

Moorman BJ and Michel FA (2000) Glacial hydrological system characterization using ground-penetrating radar. *Hydrol. Process*, **14**, 2645–2667 (doi: 10.1002/1099-1085(20001030)14:15<2645::AID-HYP84>3.0.CO;2-2)

Müller D (2007) *Incision and closure processes of meltwater channels on the glacier Longyearbreen, Svalbard*. (Masters thesis, Technische Universität Braunschweig)

Myreng SM (2015) *Characteristics and long-term evolution of an englacial meltwater channel in a cold-based glacier, Austre Brøggerbreen, Svalbard*. (Masters thesis, Norwegian University of Science and Technology)

Naegeli K, Lovell H, Zemp M and Benn DI (2014) Dendritic subglacial drainage systems in cold glaciers formed by cut-and-closure processes. *Geogr. Ann. A*, **94**(4), 591–608 (doi: 10.1111/geoa.12059)

Nienow P, Sharp M and Willis I (1998) Seasonal changes in the morphology of the subglacial drainage system, Haut Glacier d'Arolla, Switzerland. *Earth Surf. Process Landf.*, **23**, 825–843 (doi: 10.1002/(SICI)1096-9837(199809)23:9<825::AID-ESP893>3.0.CO;2-2)

Nowak A and Hodson A (2014) Changes in meltwater chemistry over a 20-year period following a thermal regime switch from polythermal to cold-based glaciation at Austre Brøggerbreen, Svalbard. *Polar Res.*, **33**(1), 22779 (doi: 10.3402/polar.v33.22779)

Osterhuber R, Howle J and Bawden G (2008) Snow measurement using ground-based tripod LiDAR. In *76th Annual Western Snow Conference*, Hood River, Oregon, 135–138

Pejić M (2013) Design and optimisation of laser scanning for tunnels geometry inspection. *Tunn. Undergr. Space Technol.*, **37**, 199–206 (doi: 10.1016/j.tust.2013.04.004)

Petrie G and Toth CK (2008) Introduction to laser ranging, profiling and scanning. In Shan J and Toth CK eds. *Topographic laser ranging and scanning principles and processing*. CRC Press, Boca Raton, 1–28

Pfiefer N and Briese C (2007) Laser scanning – principles and applications. *GeoSiberia*. In *International Exhibition and Scientific Congress*

Phillips T, Rajaram H and Steffen K (2010) Cryo-hydrologic warming: a potential mechanism for rapid thermal response of ice sheets. *Geophys. Res. Lett.*, **37**(20), 1–5 (doi: 10.1029/2010gl044397)

Picard G, Libois Q and Arnaud L (2016) Refinement of the ice absorption spectrum in the visible using radiance profile measurements in Antarctic snow. *Cryosphere*, **10**(6), 2655–2672 (doi: 10.5194/tc-10-2655-2016)

Piccini L, Romeo A and Badino G (2002) Moulins and marginal contact caves in the Gornergletscher, Switzerland. *Nimbus*, **23–24**, 94–99

Porter PR, Vatne G, Ng F and Irvine-Fynn TDL (2010) Ice-marginal sediment delivery to the surface of a high-Arctic glacier: Austre Brøggerbreen, Svalbard. *Geogr. Ann. A*, **92**(4), 437–449 (doi: 10.1111/j.1468-0459.2010.00406.x)

Prokop A (2008) Assessing the applicability of terrestrial laser scanning for spatial snow depth measurements. *Cold Reg. Sci. Technol.*, **54** (3), 155–163 (doi: 10.1016/j.coldregions.2008.07.002)

Pulina M (1984) Glacierkarst phenomena in Spitsbergen. *Norsk Geogr. Tidsskr*, **38**(3–4), 163–168 (doi: 10.1080/00291958408552121)

Resop JP and Hession WC (2010) Terrestrial laser scanning for monitoring streambank retreat: comparison with traditional surveying techniques. *J. Hydraul. Eng.*, **136**(10), 794–798 (doi: 10.1061/(ASCE)HY.1943-7900.0000233)

Robert McNeel & Associates (2017) *Rhino3d software*, Vol, **5**. Robert McNeel & Associates, Barcelona

Schaffhauser A, and 6 others (2008) Remote sensing based retrieval of snow cover properties. *Cold Reg. Sci. Technol.*, **54**(3), 164–175 (doi: 10.1016/j.coldregions.2008.07.007)

Schoof C (2010) Ice-sheet acceleration driven by melt supply variability. *Nature*, **468**(7325), 803–806 (doi: 10.1038/nature09618)

Smith MW (2015) Section 2.1.5. Direct acquisition of elevation data: terrestrial laser scanning. In Cook SJ, Clarke LE and Nield JM eds. *Geomorphological techniques (online edition)*. British Society for Geomorphology, London

Smith MW and 6 others (2016) Aerodynamic roughness of glacial ice surfaces derived from high-resolution topographic data. *J. Geophys. Res.-Earth*, **121**, 748–766 (doi: 10.1002/2015JF003759)

Soudarissanane S (2016) *The geometry of Terrestrial Laser Scanning: Identification of errors, modeling and mitigation of scanning geometry*. (Doctoral thesis, Technische Universiteit Delft)

Soudarissanane S, Lindenbergh R and Gorte B (2008) Reducing the error in terrestrial laser scanning by optimizing the measurement set-up. In *ISPRS Congress XXXVII*, Beijing, 37 (B5), 615–620

Soudarissanane S, Lindenbergh R, Menenti M and Teunissen P (2011) Scanning geometry: influencing factor on the quality of terrestrial laser scanning points. *Int. Soc. Photogramme*, **66**(4), 389–399 (doi: 10.1016/j.isprsjprs.2011.01.005)

Stuart G (2003) Characterization of englacial channels by ground-penetrating radar: an example from Austre Brøggerbreen, Svalbard. *J. Geophys. Res.*, **108**(B11) 2525 (doi: 10.1029/2003jb002435)

Tedesco M (2015) Electromagnetic properties of the components of the cryosphere. In Tedesco M ed. *Remote sensing of the cryosphere*. pp. 17–30, John Wiley & Sons, Ltd., Chichester (doi: 10.1002/9781118368909.ch2)

Vatne G (2001) Geometry of englacial water conduits, Austre Brøggerbreen, Svalbard. *Norsk Geogr. Tidsskr*, **55**(2), 85–93 (doi: 10.1080/713786833)

Vatne G and Irvine-Fynn TDL (2016) Morphological dynamics of an englacial channel. *Hydrol. Earth Syst. Sci*, **20**(7), 2947–2964 (doi: 10.5194/hess-20-2947-2016)

Vatne G and Refsnes I (2003) Channel pattern and geometry of englacial conduits. In 6th *International Symposium 'Glacier caves and karst in Polar Regions'*, Ny-Ålesund, Svalbard, 181–188

Vosselman G and Maas H-G (2010) *Airborne and terrestrial laser scanning*. Whittles Publishing, Caithness

Warild A (2007) Surveying. *Vertical*, eBook, Cavediggers.com
Warren SG (1982) Optical properties of snow. *Rev. Geophys.*, **20**(1), 67–89 (doi: 10.1029/RG020i001p00067)
Warren SG and Wiscombe WJ (1981) A model for the spectral albedo of snow. II: snow containing atmospheric aerosols. *J. Atmos. Sci.*, **37**, 2734–2745 (doi: 10.1175/1520-0469(1980)037<2734:AMFTSA>2.0.CO;2)
Wehr A (2008) LIDAR: airborne and terrestrial sensors. In Li Z, Chen J and Baltsavias EP, eds. *Advances in photogrammetry, remote sensing and spatial information sciences: 2008 ISPRS congress book*. Taylor & Francis Group, London, 73–84
Willis IC, Sharp MJ and Richards KS (1990) Configuration of the drainage system of Midtdalsbreen, Norway, as indicated by dye-tracing experiments. *J. Glaciol.*, **36**(122), 89–101 (doi: 10.1017/s0022143000005608)
Zwally HJ, Abdalati W, Herring T, K L, Saba J and Steffen K (2002) Surface melt-induced acceleration of Greenland Ice-sheet flow. *Science*, **297**, 218–222 (doi: 10.1126/science.1072708)

MS received 3 July 2017 and accepted in revised form 20 November 2017; first published online 20 December 2017